Dynamics of Spacecraft Charging by Electron Beams

M. J. Mandell and I. Katz

S-CUBED Division of Maxwell Laboratories, La Jolla, California

When a spacecraft or rocket emits an electron beam into an underdense plasma, it can charge to potentials in excess of the beam energy. We show calculations in which 8 keV beams are emitted along and across the earth's magnetic field, with parameters appropriate to the MAIMIK rocket. As was observed on MAIMIK, the spacecraft charged to potentials in excess of the beam potential due to energization of beam electrons by beam-generated electrostatic oscillations. This is in contrast to the low levels of charging often seen in denser environments, where higher plasma currents, coupled with ionization of neutrals, hold spacecraft potentials below a few hundred volts.

The beam structure and the spacecraft potential oscillate at a frequency corresponding to the mean lifetime of the beam electrons. These oscillations energize the beam electrons, and also pump energy into the ambient plasma, which exhibits lower frequency oscillations. The peak spacecraft potential is over 1 kV in excess of the beam energy. For the cross-field case, the oscillation frequency is proportional to the beam current for sufficiently intense beams.

Following beam turn-off, there is an immediate return of unscattered beam electrons and a longer term dissipation of scattered beam electrons. Analytic estimates are presented for the decay and overshoot of the spacecraft potential.

INTRODUCTION

A number of electron beam experiments have measured results that apparently violate conservation of energy. The SEPAC experiment (Reasoner *et al.*, 1984) measured a spectrum of returning electrons extending to energies well above that of the emitted beam, and the MAIMIK rocket (Maehlum *et al.*, 1988; Denig, Maehlum and Svenes, this conference) was charged by an 8 keV electron beam to potentials as high as 14 keV. Katz *et al.* (1986) performed a planar calculation that showed that oscillations of the beam electrons led to the spectral broadening seen in the SEPAC experiment. In this paper, we show 2-dimensional calculations, with parameters appropriate to MAIMIK, illustrating that space charge oscillations associated with the electron beam lead to rocket potentials in excess of the beam energy.

The electron beam on MAIMIK was directed nearly across the earth's magnetic field. The geometry of an intense beam directed across a magnetic field is shown in Figure 1a. If the spacecraft is near the beam energy, the beam electrons will be slowest at their farthest excursion from the spacecraft and will form a space charge maximum. This space charge maximum breaks the azimuthal symmetry of the problem, so that electrons may be scattered from their original gyro-orbits and leave the vicinity of the spacecraft. Unfortunately, this is a truly 3-dimensional situation and, therefore, very difficult to model.

Two beam configurations that can be modeled in 2-dimensional axisymmetric geometry are shown in Figures 1b and 1c. Figure 1b shows a beam directed along the magnetic field. An intense virtual cathode is formed. Most of the beam electrons move outward

from the virtual cathode and are attracted back to the spacecraft, which they impact from behind. A few of the beam electrons continue along the magnetic field line and escape the vicinity of the spacecraft. Figure 1c illustrates an "equatorial" beam, in which electrons are directed across the magnetic field from the entire spacecraft circumference. A ring of maximum space charge appears around the spacecraft. Because the space charge maximum is a full ring rather than a localized region, we expect it to be less intense than would be the case for a physical beam of the same current. Also, the space charge maximum is less effective at scattering because it does not break azimuthal symmetry.

The calculations described here were performed using an S-CUBED-developed, finite-element, electrostatic particle-in-cell code named Gilbert. Gilbert is a flexible, multi-purpose code with many special features. For these calculations, the space around the spacecraft was gridded with biquadratic elements of variable resolution to a distance of ten meters. Each element represents a volume of space corresponding to its area revolved in a full circle about the symmetry axis. For the "equatorial" beam, the calculation took advantage of mirror symmetry about the equatorial plane. The computational grids for the two cases are shown in Figure 2.

PHYSICAL PARAMETERS

Table 1 shows the physical parameters used in the calculation. The parameters listed in the "current collection" category are calculated for a spherical spacecraft at the beam potential of 8,000 volts.

Table 1. Problem Parameters

Geometrical Parameters	
Inner (spacecraft) Radius	0.3 m
Outer Radius	10.0 m
Magnetic Field	0.4 gauss
Beam Parameters	
Beam Current	0.16 amperes
Beam Energy	8000 eV
Plasma Parameters	
Electron/Ion Density	3×10^9 m^{-3}
Electron Temperature	1 eV
Ion Mass	16 amu
λ_D	13.6 cm
ω_{pe}	3.1×10^6 sec^{-1}
ω_{ce}	7.0×10^6 sec^{-1}
J_{th}	8.0×10^{-5} A-m^{-2}
Current Collection	
Langmuir-Blodgett Radius	10 m
Parker-Murphy Radius	1.54 m
Parker-Murphy Current	0.0025 amperes
Probe Charge	2.7×10^{-7} coulombs

The plasma surrounding the spacecraft is "underdense", in the sense that the Parker-Murphy bound (Parker and Murphy, 1967) on the plasma return current is only a few percent of the beam current. Also, the electron plasma frequency is below the electron cyclotron frequency and, as we shall see, well below the oscillation frequency of the beam.

The radius of the computational space is taken equal to the radius of a space-charge-limited spherical sheath in this plasma, which is far larger than the Parker-Murphy radius for current collections. The effect of the plasma external to this radius is represented by a zero potential condition on this boundary. In retrospect, this approximation appears adequate to represent the beam dynamics, the ion dynamics, and the collection of ambient electrons but omits long-range transient effects on the ambient electron density.

CALCULATION FOR BEAM ALONG FIELD

The calculation begins with the grid of Figure 2a filled with electron and ion macroparticles (Figure 3a). The beam is projected along the magnetic field (Figure 3b) and initially exits the computational space. The negative beam charge and the positive charge left behind on the spacecraft produce a dipole potential (Figure 3c) that expels ambient electrons from the beam region (Figure 3d).

The spacecraft reaches beam potential about 2.5 microseconds after beam turn-on (Figure 4a), and the potential exhibits persistent oscillations (at 2 x 10^6 Hz) for the duration of the calculation (Figure 4b). During this time, the spacecraft remains always above the beam potential and has a peak potential of about 9,100 volts.

The beam conformation oscillates along with the spacecraft potential. Figure 5a shows the beam conformation when the spacecraft potential is fairly high. The bulk of the beam electrons are far from the spacecraft, having been emitted when the potential was low. Figure 5b shows beam conformation at a fairly low potential. In this case, the bulk of the beam electrons are close to the spacecraft, having been emitted at high potential. However, a pulse of energized electrons can be seen escaping along the field line.

Figures 6a and 6b show the electrostatic potential structure about the spacecraft. The sheath is elongated along the magnetic field due to quasi-trapping of ambient electrons that cannot be collected. The contours are distorted along the axis by the beam electron space charge (Figure 6a). At times, a negative potential well forms in the cross-field region (Figure 6b).

Figure 7a shows the amount of beam electron charge in the computational space, and Figure 7b shows the time dependence of the dipole moment of the beam electrons, defined as

$$\text{Dipole Moment} = \int \rho \, z \, d^3\mathbf{r}$$

where ρ is the charge density of beam electrons. Since the dipole moment is oscillating at 2 MHz, we expect to see strong electromagnetic radiation at this frequency.

Figures 8abc show spectral analysis of some of the oscillating quantities. The potential (Figure 8a) shows a sharp peak at 2 MHz, with well-defined second and third harmonics. The beam dipole moment (Figure 8b) shows a sharp peak at 2 MHz, as well as a broad peak at the ambient electron plasma frequency (0.5 MHz). The dipole moment of the

ambient electrons (Figure 8c) shows little evidence of the 2 MHz oscillations but has a strong, broad peak near the ambient plasma frequency.

The beam charge (Figure 7a) varies from 0.04 to 0.08 μcoul. Dividing this by the beam current of 0.16 amperes shows that beam particle lifetimes fall mainly in the range 0.25 - 0.5 μsec. Noting also that the upstrokes in Figure 7a (strong return current) are steeper than the downstrokes (steadily emitted current) leads to the following interpretation. Most of the beam electrons return to the spacecraft in a short burst. Electrons emitted during the return burst see relatively weak retarding fields, travel far from the spacecraft, and have lifetimes of approximately a full oscillation period. Electrons emitted while the potential is rising see stronger retarding fields, travel smaller excursions, and return to the spacecraft at the same time as the long-lived electrons, producing the return current bunching. This bunching is similar to that seen by Katz *et al.* (1986).

Figure 9 shows the ion positions at the conclusion of the calculation (20 μsec). The ions have cleared a region of about two meters around the spacecraft. Thus the run time of this calculation is too short to approach the formation of an equilibrium "sheath".

CALCULATION FOR BEAM ACROSS FIELD

A similar calculation was performed for an equatorial beam directed across the magnetic field in the grid of Figure 2b. (Note that in this calculation we have taken advantage of mirror symmetry about the z = 0 plane. Values for current and charge will be quoted at double the computed values, so that they are characteristic of a complete sphere.)

The beam electrons at the conclusion of the calculation are shown in Figure 10. The figure shows a main stream of electrons emitted from the spacecraft, slowed by the electric field and turned by the magnetic field, then returning to the spacecraft. In addition, there is a column of beam electrons extending in the magnetic field direction. The mechanism for populating this column is that a beam electron in its initial orbit gains enough momentum along the magnetic field to miss the spacecraft on its first return passage, and while passing near the spacecraft receives a substantial impulse along the field. Electrons leave the column by either impacting the spacecraft or escaping the grid.

Figures 11ab show the time history of the spacecraft potential. Four different current values were used. From Figure 11b we see that, while doubling the current led to some increase in the mean potential and its oscillation amplitude, the main effect is to double the frequency.

Figures 12ab show the potential contours about the spacecraft at two different times. As in the previous case, the sheath is elongated along the field line, and a negative potential well is sometimes seen in the cross-field region.

Figure 13 shows the ambient electron macroparticles. The ambient electron population was maintained by generating the plasma thermal current at the spherical problem boundary out to a radius of eight meters. A low density region is seen to extend along the field line from the spacecraft; electrons in this region are allowed by the theory of Parker and Murphy (1967) to be collected by the spacecraft. A high-density cloud of electrons is seen in the cross-field region, as these electrons cannot be collected by the spacecraft and have low probability of escaping the grid. This ambient electron charge density structure is the cause of the elongated potential contours shown in Figures 12ab and 6ab.

Table 2 shows the range of beam charge, range of beam electron lifetime, and oscillation period for the different values of emission current. As with the field-aligned beam, the oscillation period is near the maximum beam particle lifetime. Except for the lowest current value, the beam charge increases only slightly when the current is doubled. This is because the maximum beam charge is approaching the charge on the sphere. When the current is doubled, a modest increase in mean spacecraft potential is sufficient to reduce the particle excursion distance and cut the beam particle lifetime by half. This point is further illustrated by Figure 14, which plots the quantity

$$\int \rho \, r \, d^3r$$

The average and oscillation amplitude of this quantity varies slowly as the sheath is being formed, but shows no abrupt changes as the current is altered, leading to the conclusion that the system rapidly adjusts so that the beam charge times its excursion distance is independent of current.

Table 2. Beam Charge, Lifetime, and Oscillation Period for Equatorial Beam

Current (Amperes)	Charge (μcoul)	Lifetime (μsec)	Period (μsec)
0.16	0.07 - 0.1	0.44 - 0.62	0.62
0.32	0.12 - 0.2	0.38 - 0.62	0.47
0.64	0.13 - 0.21	0.20 - 0.33	0.28
1.28	0.14 - 0.25	0.11 - 0.19	0.18

BEAM TURN-OFF

Several papers at this conference discussed beam turn-off, showing that the spacecraft potential tends to overshoot and achieve a negative value. This led us to investigate the behavior of the equatorial beam system after turn-off of the 0.160 ampere beam.

Figure 15 shows the behavior of the spacecraft potential and the beam charge following beam turn-off. Most of the beam charge is promptly collected, dropping the spacecraft potential to 7,200 volts. Approximately 0.03 μcoul of charge remains in the field-aligned column of scattered beam electrons, which decays with a time constant of 2.1 μsec. About three-quarters of this depopulation rate results from electrons escaping the grid, and about one-quarter from electrons recaptured by the spacecraft. (When the spacecraft is at elevated potential, the escape rate must balance the Parker-Murphy collected current, leading to a 12 μsec time constant for escape.)

If the spacecraft discharges by collecting the Parker-Murphy current, its potential will follow the equation

$$dV/dt = (I_0/C)\,(V/V_0)^{1/2}$$

where I_0 is the Parker-Murphy current at potential V_0 (- 0.0025 amperes at 8,000 volts) and C is the spacecraft capacitance (3.4×10^{-11} farads). The solution is

$$t_2 - t_1 = -2.4 \times 10^{-6}\,(V_2^{1/2} - V_1^{1/2})$$

which gives a discharge time of about 200 μsec. Since the thermal ion speed is only a few thousand m-sec^{-1}, it will take about a millisecond for the ions to repopulate a sheath a few meters in radius. Assuming a thermal electron distribution, the spacecraft will charge negatively during this time according to

$$dV/dt = 4\pi a^2 J_{th}\, e^{V/\theta} / C$$

whose solution is

$$V/\theta = -\ln(1 + t/\tau)$$
$$\tau = C\,\theta / (4\pi a^2 \mid J_{th} \mid)$$

For our parameters, τ is about 0.4 μsec, and we expect an overshoot to about -8 volts. However, if the electron distribution has an elevated thermal tail, as is likely due to turbulence associated with the nonuniform, nonequilibrium ion distribution, the negative overshoot will be much greater.

CONCLUSIONS

Electron beams emitted from spacecraft in the ionosphere exhibit complex behavior. We have analyzed here the case of a beam emitted into an underdense plasma, with parameters appropriate to the MAIMIK rocket. The beam was emitted both along the magnetic field and across the field in an "equatorial" fashion.

The beam-emitting system exhibits oscillations at a few megahertz. These oscillations are associated with bunched return of the beam electrons and cause electron energization so that the spacecraft can achieve potentials in excess of the beam energy. At least for the field-aligned beam case, these oscillations are dipolar in character and should be observable as electromagnetic radiation. For sufficiently intense beams, the oscillation frequency is proportional to the beam current.

The dynamics of the ambient plasma is largely independent of the beam dynamics. The ambient electrons show a broad peak at their own plasma frequency and form an elongated sheath.

Even in this very underdense plasma, the relaxation of spacecraft potential following beam turn-off is rapid compared with the time for ions to thermally fill in the sheath. If the nonuniform plasma that exists during this time causes electron heating, a substantial negative overshoot of the spacecraft potential can occur.

Acknowledgement. This work was supported by the Geophysics Laboratory, Hanscom Air Force Base, Massachusetts, under contract F19628-89-C-0032.

REFERENCES

Denig, W. F., B. N. Maehlum, and K. Svenes, A review of the MAIMIK rocket experiment, (this conference, 1989).

Katz, I., G. A. Jongeward, D. E. Parks, D. L. Reasoner and C. K. Purvis, Energy broadening due to space-charge oscillations in high current electron beams, *Geophy. Res. Lett.*, *13*, 64, 1986.

Maehlum, B. N., J. Troim, N. C. Maynard, W. F. Denig, M. Friedrich, and K. M. Torkar, Studies of the electrical charging of the tethered electron accelerator mother-daughter rocket MAIMIK, *Geophy. Res. Lett.*, *15*, 725, 1988.

Parker, L. W., and B. L. Murphy, Potential buildup on electron-emitting ionospheric satellites, *J. Geophys. Res.*, *72*, 1631, 1967.

Reasoner, D. L., J. L Burch, and T. Obayashi, Analysis of electron spectra produced by SEPAC electron beams on Spacelab-1 - evidence for strong beam plasma interactions, *EOS, Trans. Am. Geophys Union* , *65*, 1042, 1984.

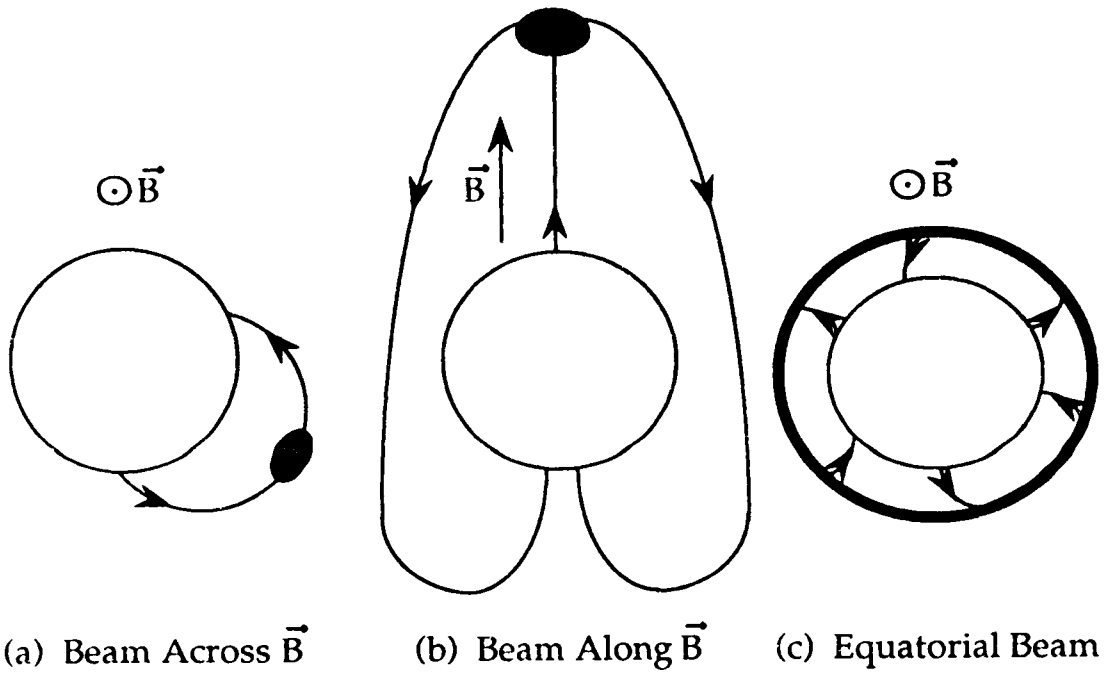

Fig. 1. Three beam configurations from a spherical spacecraft: (a) physical beam across magnetic field; (b) physical beam along magnetic field; (c) "equatorial" beam across magnetic field.

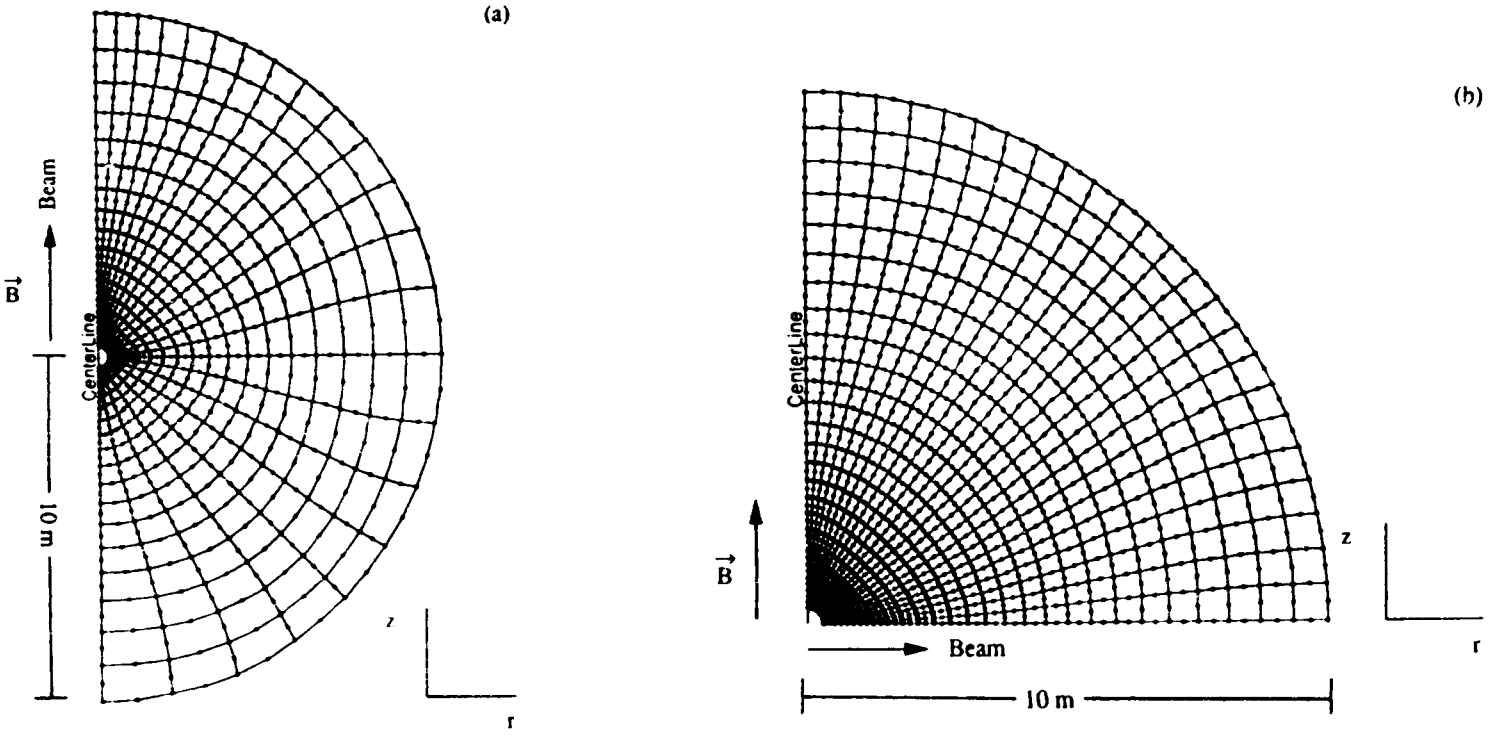

Fig. 2. Axisymmetic grids of biquadratic elements used in these calculations: (a) grid used for calculation of beam along magnetic field (fig. 1a); (b) grid used for calculation of "equatorial" beam (fig. 1b) using mirror plane.

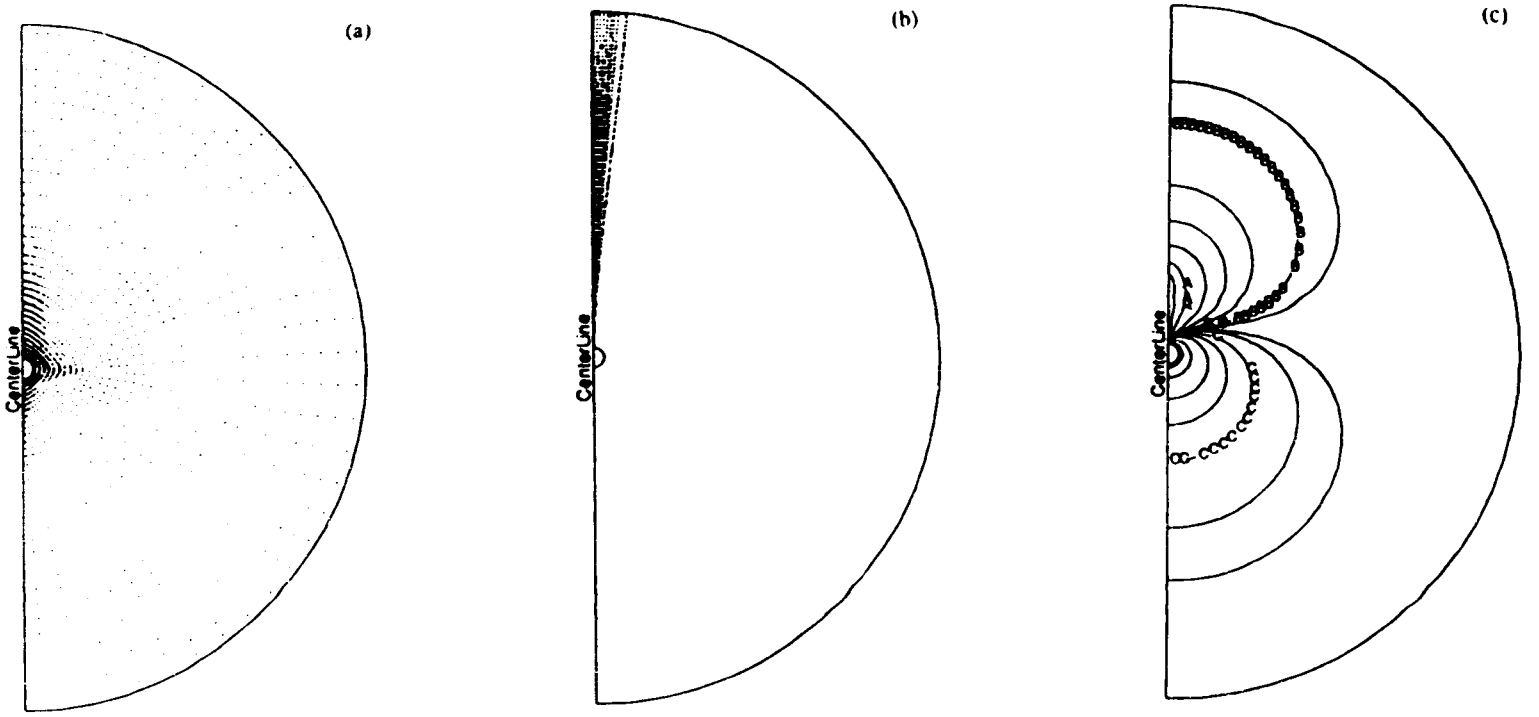

Figure 3. (a) Initial electron or ion macroparticles in grid of fig. 2a; (b) beam electron macroparticles at 0.2 μsec; (c) dipolar potential at 0.04 μsec, with contours marked A, B, and C at -50, -2, and +5 volts.

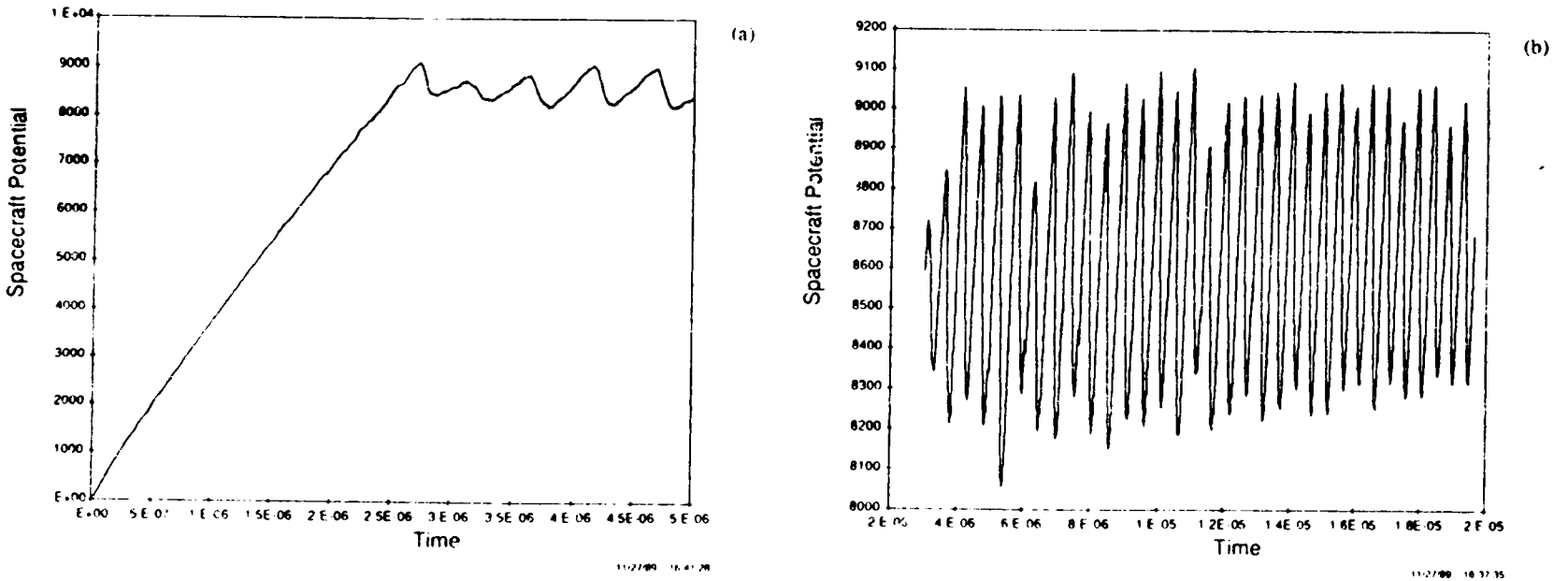

Fig. 4. Time dependence of spacecraft potential for field-aligned beam: (a) initial transient; (b) persistent oscillations.

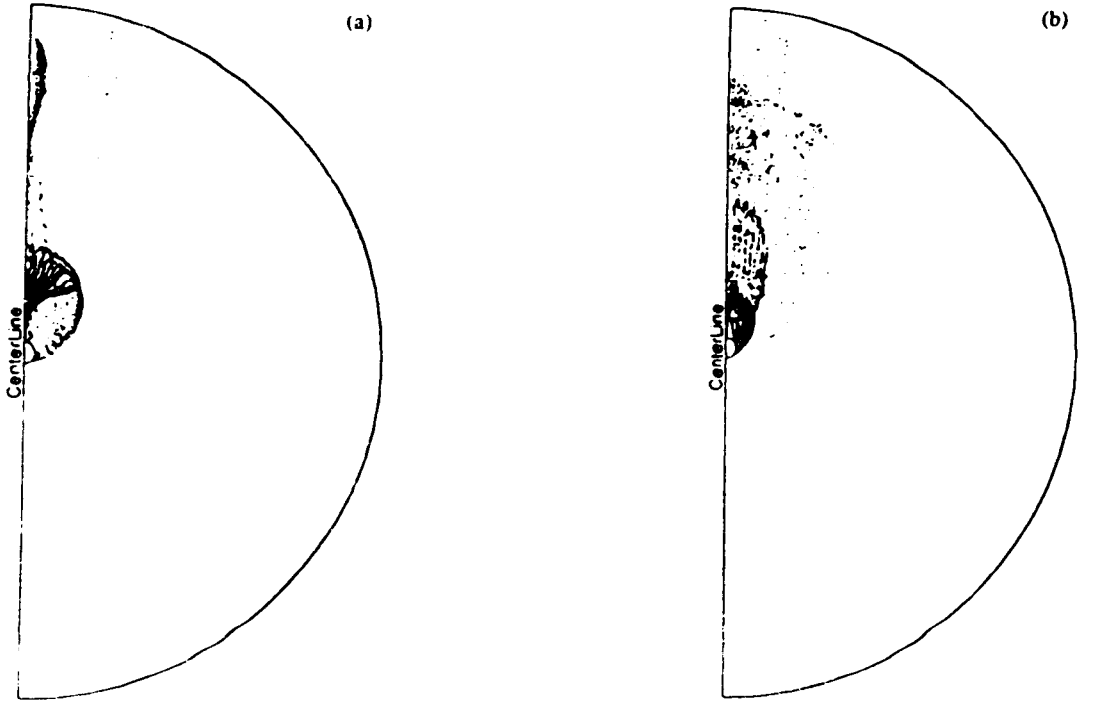

Fig. 5. Beam conformation (a) at high potential; (b) at low potential.

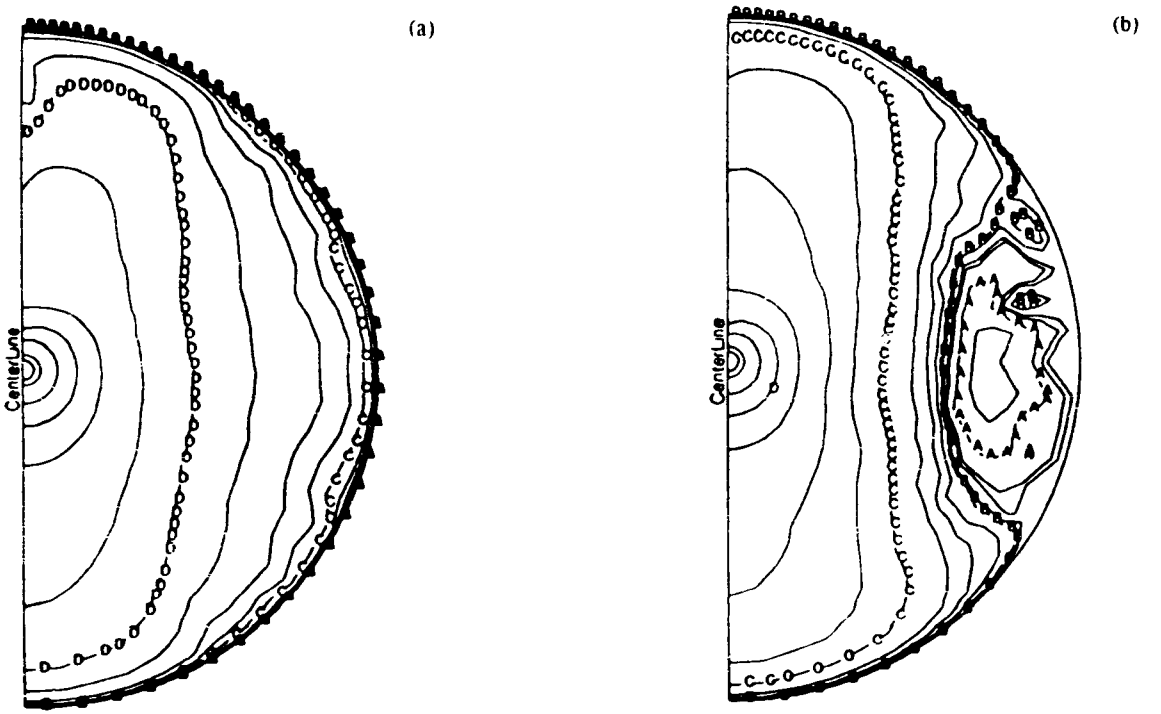

Fig. 6. Electrostatic potential structure (logarithmically spaced contours) about the spacecraft (a) without and (b) with negative potential well in the cross-field region.

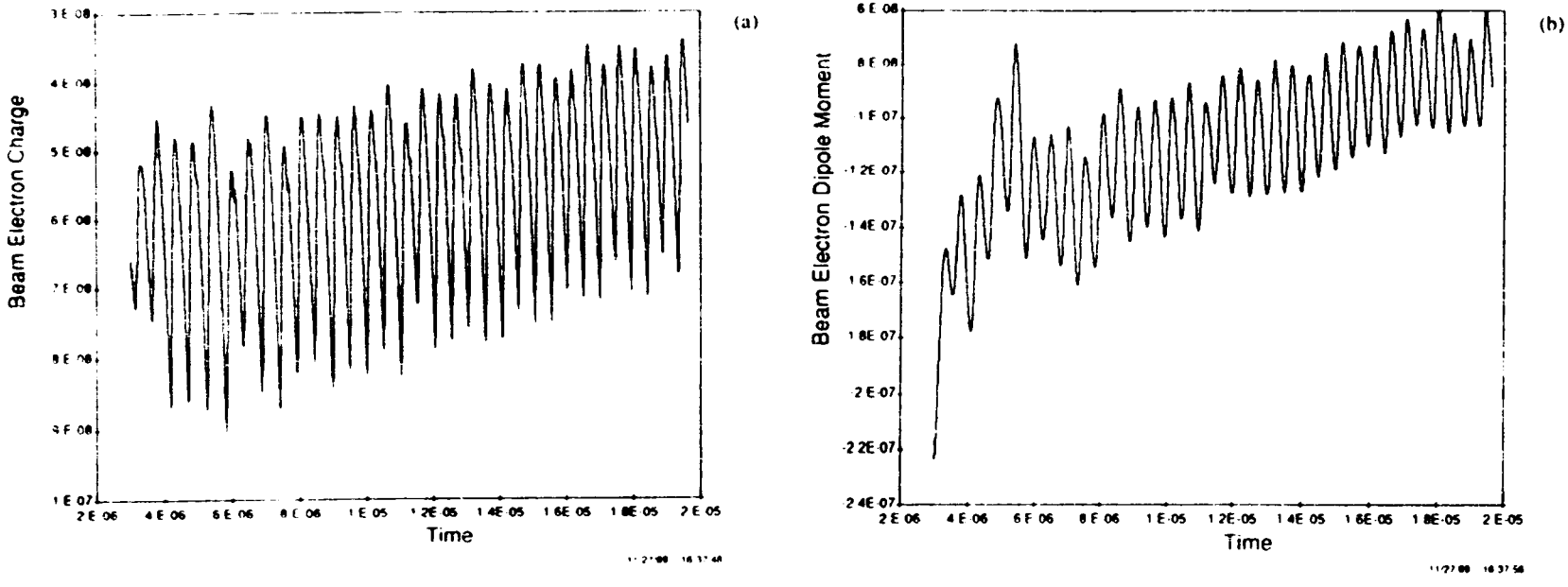

Fig. 7. Time dependence of (a) beam electron charge; and (b) beam electron dipole moment.

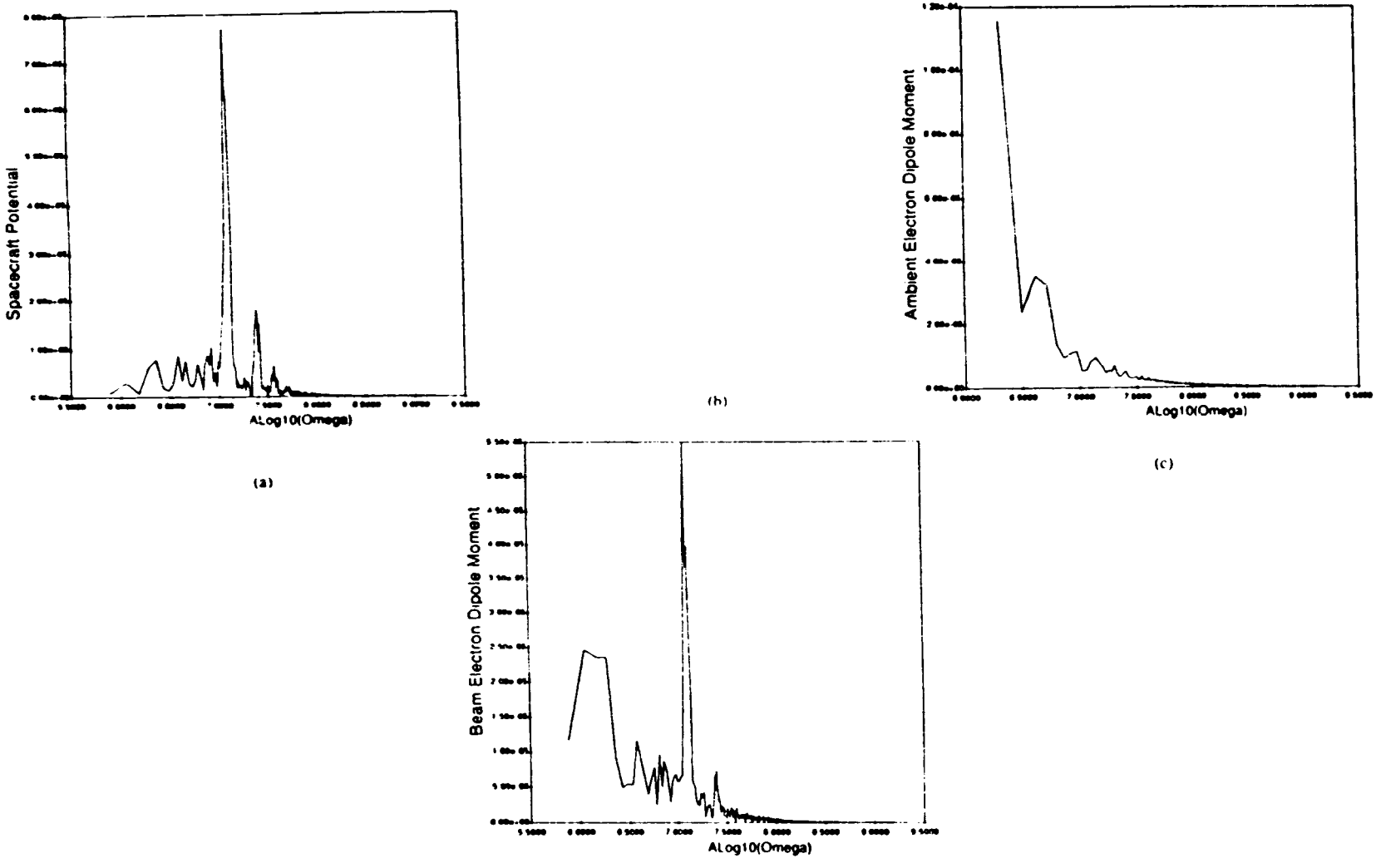

Fig. 8. Spectral analysis of (a) spacecraft potential; (b) beam electron dipole moment; (c) ambient electron dipole moment.

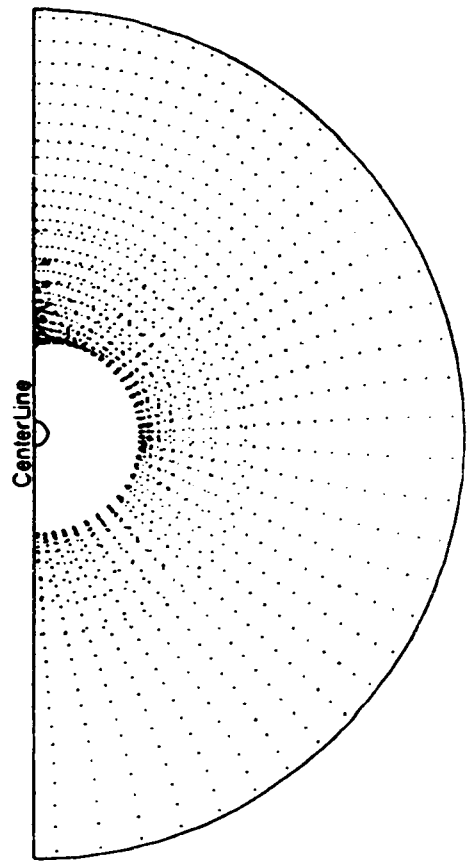

Fig. 9. Ion positions after 20 μsec.

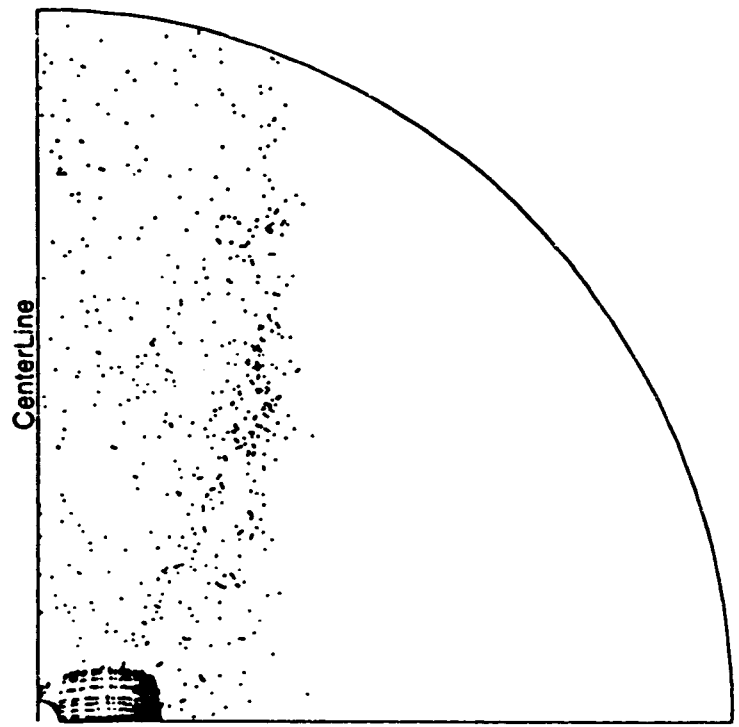

Fig. 10. Beam electrons at conclusion of equatorial beam calculation, showing circulating beam of unscattered electrons, and field aligned column of scattered electrons.

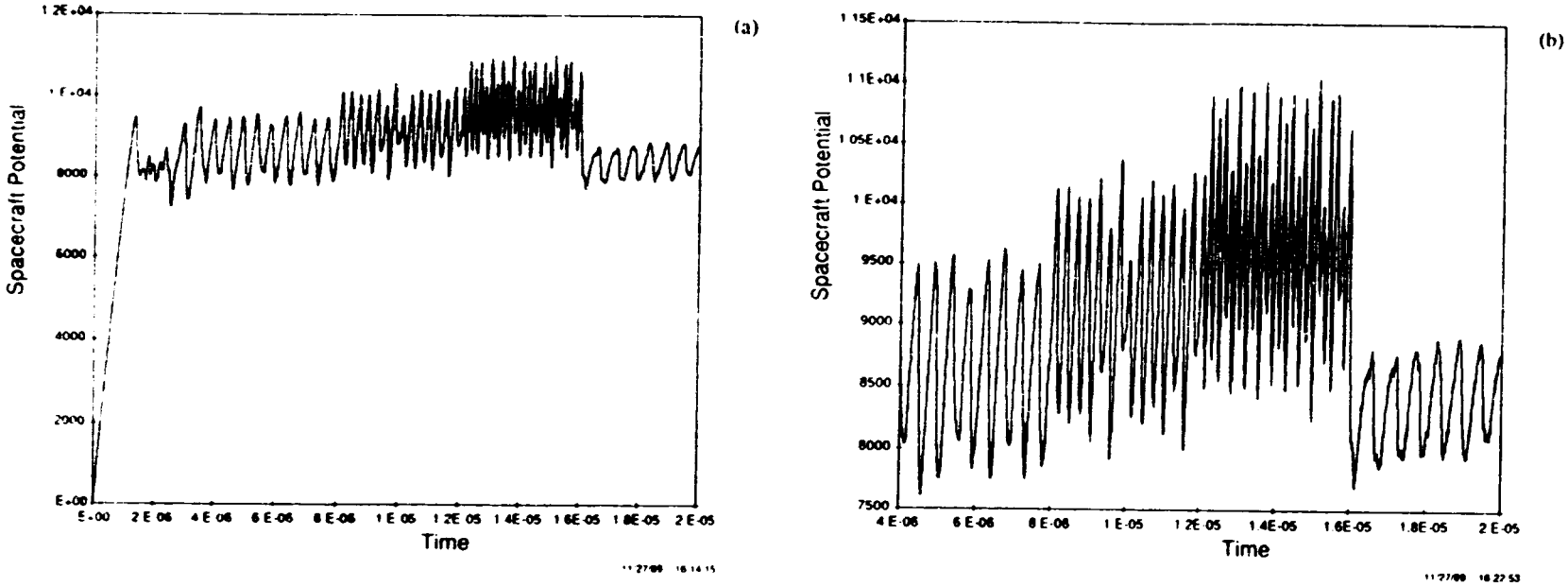

Fig. 11. Time dependence of spacecraft potential for equatorial beam: (a) initial transient; (b) persistent, current-dependent oscillations.

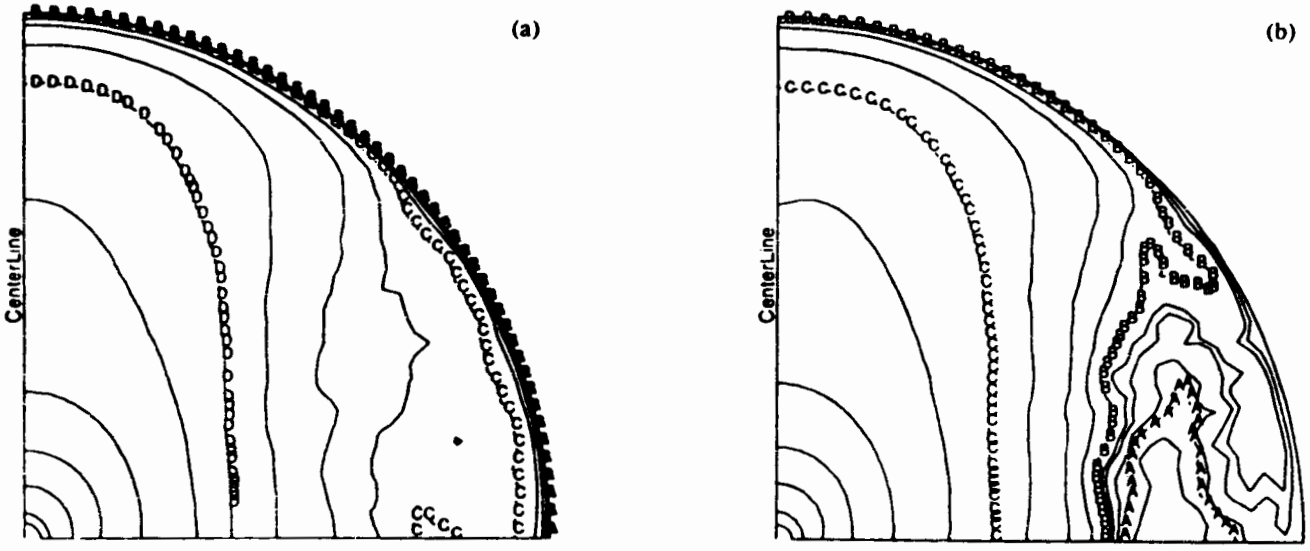

Fig. 12. Electrostatic potential structure (logarithmically spaced contours) about the spacecraft (a) without and (b) with negative potential well in the cross-field region.

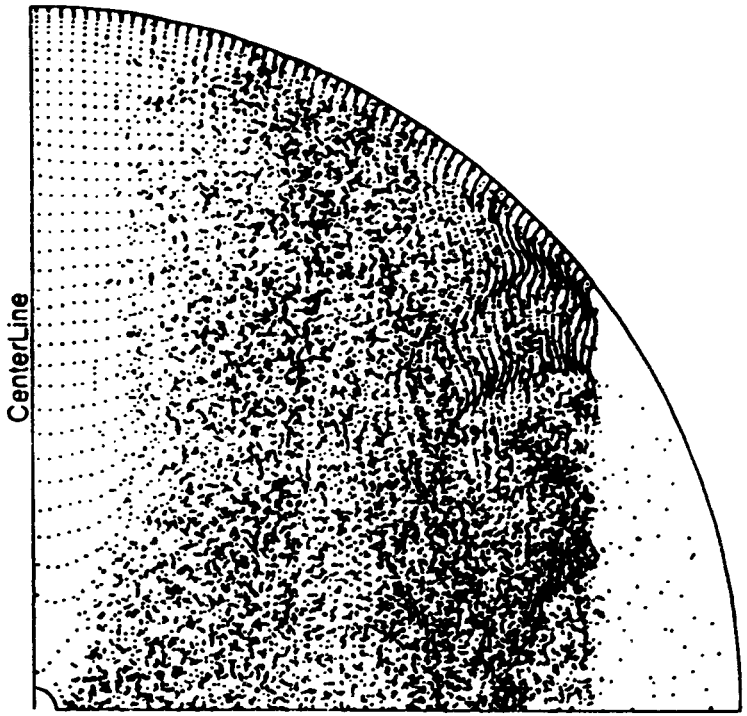

Fig. 13. Ambient electron macroparticles, showing low axial density and high cross-field density.

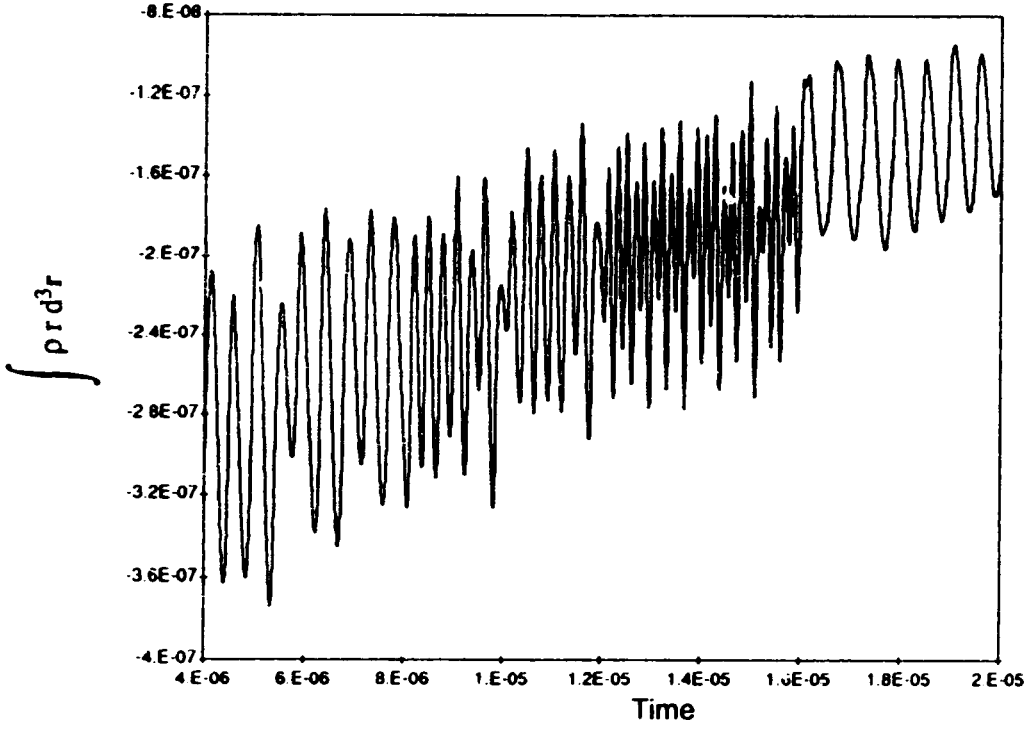

Fig. 14. The quantity $\int \rho\, r\, d^3\mathbf{r}$ for the beam electrons, showing the lack of dependence on strong current changes.

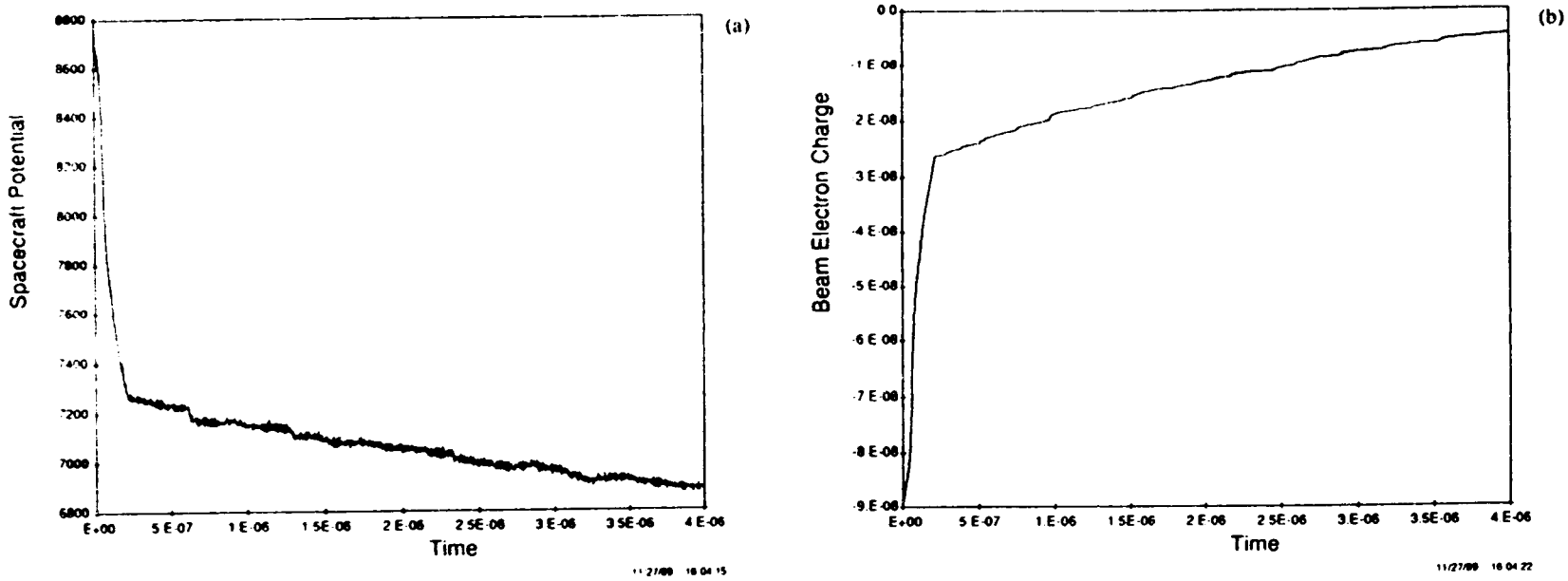

Fig. 15. Behavior following beam turn-off: (a) spacecraft potential; (b) beam electron charge.